

INTERMEDIATE-MASS BLACK HOLE(S) AND STELLAR ORBITS IN THE GALACTIC CENTER

YURI LEVIN, ALICE WU, AND ED THOMMES

Canadian Institute for Theoretical Astrophysics, 60 St. George Street, Toronto, ON M5S 3H8, Canada

Draft version August 29, 2018

ABSTRACT

Many young stars reside within the central half-parsec from SgrA*, the supermassive black hole in the Galactic Center. The origin of these stars remains a puzzle. Recently, Hansen and Milosavljevic (2003, HM) have argued that an Intermediate-Mass Black Hole (IMBH) could have delivered the young stars to the immediate vicinity of SgrA*. Here we focus on the final stages of the HM scenario. Namely, we integrate numerically the orbits of stars which are initially bound to the IMBH, but are stripped from it by the tidal field of SgrA*. Our numerical algorithm is a symplectic integrator designed specifically for the problem at hand; however, we have checked our results with SYMBA, a version of the widely available SWIFT code. We find that the distribution of the post-inspiral orbital parameters is sensitive to the eccentricity of the inspiraling IMBH. If the IMBH is on a circular orbit, then the inclinations of numerically computed orbits relative to the inspiral plane are almost always smaller than 10 degrees, and therefore (a) the simulations are in good agreement with the observed motions of stars in a clockwise-moving stellar disc, (b) the simulations never reproduce the orbits of stars outside this disc, which include those in the second thick ring of stars and the randomly oriented unrelaxed orbits of some of the S-stars. If the IMBH's orbital eccentricity is $e = 0.6$, then approximately half of the stars end up with orbital inclinations below 10 degrees, and another half have inclinations anywhere between 0 and 180 degrees; this is somewhat closer to what's observed. We also show that if IRS13 cluster is bound by an IMBH, as has been argued by Maillard et. al. 2004, then the same IMBH could not have delivered all of the young stars to their present location.

Subject headings: black holes, massive stars, orbits

1. INTRODUCTION

A few tens of bright, young, and massive stars have been observed in close proximity (0.001—0.5 pc) to the radio source SgrA*, which is associated with the supermassive ($4 \times 10^6 M_\odot$) black hole in the Galactic Center¹ (see Genzel et. al. 2000, Ghez et. al. 2003, Shodel et. al. 2002, 2003 for recent work). The apparent youth of these stars implies two logical possibilities for their birth history: (1) either they were born *in situ*, in the immediate vicinity of SgrA*, or (2) they were born some distance away and then delivered to SgrA* within a few million years after their birth. In the first scenario, the *in situ* birth would occur in a strong tidal field of SgrA*, and the density of the star-forming gas would have to be several orders of magnitude greater than that anywhere else in the Galaxy (Phinney 1989, Sanders 1992, Morris 1993). The most likely geometry for the star-forming gas is a dense disc, which is either compressed by the central explosion powered by SgrA* (Morris, Ghez, and Becklin 1999), or, more plausibly, which is massive enough to become self-gravitating and fragment into stars² (Levin and Beloborodov 2003, Nayakshin, Cuadra, and Sunyaev 2004, Milosavljevic and Loeb 2004, Nayakshin and Cuadra 2004). The *in situ* formation is not the focus of this paper, although we will briefly return to it in our concluding remarks.

The second scenario, which is the focus of this paper, calls for rapid delivery of the young stars to the supermassive Black Hole. The initial version of it was proposed by Gerhard 2001, and investigated in more detail by McMillan and Portegies Zwart 2003, and Kim and Morris 2002. Gerhard's basic idea was that if a massive ($\sim 10^6 M_\odot$) cluster of stars was born

10—30pc away from SgrA*, then the dynamical friction in the central bulge would bring the cluster towards SgrA* on the timescale of a few million years. During the inward migration, the massive stars in the cluster would sink to the cluster's center and form a compact core. Gerhard has argued that even though the envelope of the cluster gets stripped by the tidal field a few parsecs away from SgrA*, the dense cluster core would only be tidally disrupted within the central parsec. However, even that is not close enough: the observed stars reside 0.001—0.5 pc from SgrA* and the core density would have to increase by orders of magnitude before it could get so close to SgrA*.

Recently, Hansen and Milosavljevic 2003 (from now on, HM) have suggested a fix to Gerhard's scenario which would enable the stars to be delivered to the observed proximity from SgrA*. They have argued that if an Intermediate-Mass Black Hole (IMBH), with the mass of 10^3 — $10^4 M_\odot$, was positioned at the center of the cluster, than it would provide some extra gravitational binding for the cluster core. This scenario is supported by an observation of the seemingly bound mini-cluster IRS13 at ~ 0.1 pc from SgrA* (Maillard et. al. 2004, from here on MPSR). MPSR have argued that the presence of an IMBH at the center of IRS13 is the most plausible explanation of how the mini-cluster keeps itself together in the strong tidal field of SgrA*. On the theoretical side, a number of investigations argue that IMBH would plausibly form in a dense core of a young very massive cluster (Portegies Zwart et. al. 2004, Gurkan et. al. 2004). The cluster+IMBH inspiral would consist of two stages: the first one, in which most of the most of the cluster is tidally disrupted at about a parsec from SgrA* and the IMBH is released together with a few tens of massive stars tightly bound to it, and the second one, in which the IMBH con-

¹For convenience, we shall refer to the supermassive black hole simply as SgrA*.

²We note that it is by no means certain that the disc would circularize before forming stars (J. Goodman, private communications).

tinues its inspiral while the stars are peeled off one-by-one by the SgrA* tidal pull, and are eventually put into nearly Keplerian orbits around SgrA*. The first stage was recently investigated numerically by Kim and Morris 2003 (KM) and by Gurkan and Rasio 2004. KM have found that very few stars survive bound to IMBH once it gets to the central parsec. However, one of the numerical limitations in KM (pointed out by the authors) was the large softening length for gravitational interactions between the stars. Thus KM did not model faithfully the internal dynamics of the cluster. A more exact Monte-Carlo-based simulation of Gurkan and Rasio 2004 has found that the number of stars bound to IMBH at the end of the first stage is consistent with the number of young stars in the central half-parsec.

Here we focus on the second stage—the final inspiral of the IMBH. We investigate numerically the stellar orbits produced by such an inspiral, and compare them to observations. In the next section we describe the algorithm which was used for the numerical orbital integrations; this section may be skipped by a reader uninterested in technical details³. In section 3 we present our numerical results, and in section 4 compare them to the data. We find that while the inspiral on a circular orbit explains nicely the clockwise-moving stellar disc in the Galactic Center (Levin and Beloborodov 2003, Genzel et. al. 2003), it does not reproduce the thick counterclockwise stellar disc and the randomly oriented tight orbits of the S-stars (Ghez et. al. 2003, Shodel et. al. 2003). The inspiral on an eccentric orbit does push some orbits out of the inspiral plane, but is still not entirely consistent with the current data. We also show that the proposed IMBH at the center of IRS13 almost certainly could not have delivered all of the young stars to the Galactic Center. Finally, we speculate how the HM scenario may be modified to account more closely for all of the kinematic data.

2. OUR NUMERICAL ALGORITHM: SYMPLECTIC INTEGRATOR IN THE EXTENDED PHASE SPACE

The stars in our system will experience repeated close encounters with the IMBH even after they get tidally stripped from it, and we expect the resulting orbits to be very chaotic and sensitive to the initial conditions. Therefore, our study will be statistical in nature: we are seeking to find the *distribution* of orbits which are produced by the IMBH inspiral. Symplectic algorithms (SA; see Yoshida 1990) are particularly suitable for statistical studies, since they generate trajectories which conserve the phase-space volume exactly. Integrators which use SAs have excellent long-term behavior, since the Hamiltonian mapping used in a SA is integrated exactly and is only slightly different from a true Hamiltonian mapping of the system. However, for our purposes the simplest symplectic codes have a disadvantage since they do not handle well the close encounters between a star and IMBH (see Preto and Tremaine 1999 for discussion). The origin of this limitation is the reduced timestep which is used to integrate through the encounter; reduction of the timestep leads to change of the SA Hamiltonian and thus may cause spurious energy changes. To overcome this problem, Mikkola (1997), Preto and Tremaine (1999), Mikkola and Tanikawa (1999), and Mikkola and Wiegart (2002) have developed *extended phase-space* Symplectic Integrators which use fixed timestep but in an extended phase space. The basic idea for extending the phase space of the Hamiltonian system goes back to Poincare, and can be briefly described as follows:

Let $H(q, p, t)$ be a time-dependent Hamiltonian, where q and

p stand for spatial coordinates and their conjugate momenta respectively and t is the time. Let us extend the phase space of the system by another coordinate q_0 and its conjugate momenta p_0 . Consider now a new Hamiltonian Γ in the extended phase space (Mikkola 1997):

$$\Gamma(q, q_0, p, p_0) = g(q, q_0, p, p_0) [H(q, p, q_0) + p_0], \quad (1)$$

where g is some smooth differentiable function. This Hamiltonian depends only on the coordinates and momenta of the extended phasespace; thus any trajectory in the extended phase space which satisfies Hamiltonian equations will conserve Γ . Therefore, if a particle begins its motion on the hypersurface $p_0 = -H(q, p, q_0)$, it will always stay on this hypersurface. Moreover, the trajectory of this particle $[q(\tau), p(\tau), q_0(\tau)]$ will trace the values $[q, p, t]$ corresponding to the trajectory of the original Hamiltonian system; here τ is the time variable which marks evolution in the extended phase space. The two time variables are related by

$$dt = g(q, q_0, p, -H) d\tau. \quad (2)$$

The idea then is to integrate the system numerically in the extended phase space using the constant timestep $d\tau$, but choosing g so that the real timestep dt is small during a close encounter.

To integrate the motion in a symplectic way, we need the Hamiltonian Γ to be separable into two parts,

$$\Gamma = \Gamma_A + \Gamma_B, \quad (3)$$

so that the motion due to each of Γ_A and Γ_B would be integrable analytically. Once such separation is found, the system can then be integrated via a generalized leapfrog step:

$$U(d\tau) = U_A(d\tau/2)U_B(d\tau)U_A(d\tau/2), \quad (4)$$

where $U_A(d\tau)$ and $U_B(d\tau)$ represent the forward motion in the extended phasespace by the time interval $d\tau$ under the action of Γ_A and Γ_B , respectively. Preto and Tremaine 1999 and Mikkola and Tanikawa 1999 have independently found the form of the generalized Hamiltonian which is the sum of two analytically integrable parts:

$$\Gamma = f(p_0 + K) - f(-U[q, q_0]), \quad (5)$$

where K and U are the kinetic and potential energies, respectively, and f is an arbitrary smooth function. The Hamiltonian in Eq. (5) is obviously of the form in Eq. (1), with $g = \Gamma/(p_0 + K + U)$. When $p_0 = -H$, i.e. at the hypersurface representing the original Hamiltonian system, $g = f'(-U)$. The choice $f(x) = \log x$ possesses the following surprising and useful property: the generalized leapfrog step for a two-body problem follows *exactly* the correct conic-section orbit, albeit with some time error. The real time and the time in the extended phase space are then related by

$$dt = d\tau / (-U). \quad (6)$$

We can now see the advantage of using the extended phase space. In the extended phase space, we can integrate the motion by using the generalized leapfrog in Eq. (4) with the timestep fixed, which is required for energy conservation. However, the timestep in real phase space will not be constant: when the

³In our view, however, this algorithm is of interest in its own right and may be used in other contexts.

potential energy becomes large during a close encounter, the timestep in real space becomes small and the precision of real-space integration increases.

For our problem however, the generalized Hamiltonian in Eq. (5) is not optimal. We are interested in a restricted 3-body problem where a star is interacting with two much heavier Black Holes. The mass ratio between SgrA* and the IMBH is 1000 or more⁴ and our star is initially bound to IMBH. The potential energy of the star per its unit mass is given by

$$U = -\frac{M}{|\vec{r} - \vec{r}_1|} - \frac{m}{|\vec{r} - \vec{r}_2|}, \quad (7)$$

where \vec{r} is the position vector of the star, M and \vec{r}_1 are the mass and the position vector of SgrA*, and m and \vec{r}_2 are those of the IMBH. In our simulations, the star is treated as a massless particle and the orbits of the two black holes are introduced by hand, with the inspiral prescription motivated by analytical calculations. We see from Eq. (7) that the potential energy of the star is dominated by its interaction with SgrA*, even when it is well inside the Roche Lobe of the IMBH. Thus if the Hamiltonian of Eq. (5) is used to generate the integrator, the following paradoxical situation may occur: the star may be on a bound orbit around the IMBH or it may be experiencing a close encounter with the IMBH, yet the choice of timestep will be dominated by the star's interaction with SgrA* and not with the IMBH. Clearly, to make the integrator efficient, we need to reduce the relative contribution to the timestep from the star-SgrA* interaction. The following generalized Hamiltonian, found by Mikkola and Wiegert in 2002, does the trick:

$$\Gamma = \log \left(p_0 + K - \frac{1-\alpha}{|\vec{r}|} \right) - \log \left(\frac{m}{|\vec{r} - \vec{r}_2|} + \frac{\alpha}{|\vec{r}|} + \delta \right). \quad (8)$$

Here all the position vectors are measured relative to the barycenter of black-hole binary, which is very close to SgrA*, $\alpha \ll 1$ is a positive number, and the term δ is given by

$$\delta = M \times \left(\frac{1}{|\vec{r} - \vec{r}_1|} - \frac{1}{|\vec{r}|} \right). \quad (9)$$

Since we treat the star as a test particle and introduce the orbits of both black holes by hand, the vectors \vec{r}_1 and \vec{r}_2 are time-dependent and therefore are prescribed functions of q_0 . Both components of the Hamiltonian in Eq. (8) are easily integrable: the first term on the RHS describes Keplerian motion around the barycenter and the second term describes the motion where all positions stay constant and all momenta change linearly with time; therefore we can efficiently construct the generalized leapfrog operator for this Hamiltonian. The timestep in real phase space is then given by

$$dt = d\tau \times \left(\frac{m}{|\vec{r} - \vec{r}_2|} + \frac{\alpha}{|\vec{r}|} + \delta \right)^{-1} \quad (10)$$

If one chooses $\alpha = (m/M)^{2/3}$, then at the IMBH Roche surface the star-SgrA* interaction and star-IMBH interaction contribute approximately equally to the timestep, and the contribution from the δ -term is relatively small.

⁴The mass of the IMBH is limited from above by the mass of massive stars participating in the core collapse of the IMBH's parent cluster, about 0.1% of the cluster's mass.

⁵We will discuss elsewhere how we have implemented this procedure in practice.

Mikkola and Wiegert (2002) have proposed to use the generalized Hamiltonian in Eq. (8) for simulating the motion of near-Earth and near-Jupiter asteroids. They have cautioned however, that if the asteroid gets too close to the sun, the δ -term in Eq. (8) may become large, and the Hamiltonian may become singular. Our simulations have confirmed this. We have found that while for circular inspiral the Hamiltonian in Eq. (8) always works well, for an eccentric inspiral some of the simulation runs crash because the Hamiltonian becomes singular. However, we have identified a way to fix this singularity problem by a slight modification of both parts of the generalized Hamiltonian:

$$\Gamma = \log \left(p_0 + K - \frac{1-\alpha}{|\vec{r}|} + \frac{\epsilon^2}{2r^2} \right) - \log \left(\frac{m}{|\vec{r} - \vec{r}_2|} + \frac{\alpha}{|\vec{r}|} + \delta + \frac{\epsilon^2}{2r^2} \right). \quad (11)$$

The above Hamiltonian is of the form in Eq. (1) and, moreover, the two terms on the RHS are still separately integrable. The latter statement is not trivial for the first term on the RHS; however, recall that for a particle motion in a spherically symmetric potential $V(r)$ the effective potential for the radial motion is given by $V(r) + (1/2)L^2/r^2$, where L is the particle's angular momentum. Thus adding the term $(1/2)\epsilon^2/r^2$ to the Hamiltonian is equivalent to rescaling of the particle's angular momentum in the radial equation of motion: $L \rightarrow \sqrt{L^2 + \epsilon^2}$, and solving the equations of motion with this term can be reduced to solving a purely Keplerian problem⁵. It is straightforward to show that by setting the value of ϵ so that $\epsilon^2/2 > mr_2^{\max}$ one can avoid the singularity in the generalized Hamiltonian; here r_2^{\max} is the maximal distance from the IMBH to the barycenter during the simulation run.

In this work, we have used the Hamiltonians in Eq. (8) and Eq. (11) to simulate the circular and eccentric IMBH inspirals, respectively. We have also, as a check, have run test simulations with SYMBA, a version of widely available SWIFT code with the added ability to resolve close encounters between massive objects (Duncan, Levison, and Lee 1998). We have confirmed that our integrator and SYMBA give results which are consistent with each other. The efficiency of our code has allowed us to run thousands of inspiral simulations and obtain a distribution of the orbital parameters of the stars at the end of the inspiral. In the next section, we discuss the results of our simulations.

3. RESULTS

3.1. Parameters of the inspiral.

We show in the Appendix that the eccentricity of the inspiraling IMBH remains nearly constant for the observed density profile of the stellar cluster. The semimajor axis evolves with time as

$$a(t) = a_0 \exp(-t/t_0), \quad (12)$$

where t_0 is the characteristic inspiral time given by

$$t_0 = \frac{M^{1.5}}{8\pi\sqrt{G}\rho r^{1.5} \log(\Lambda)}, \quad (13)$$

where M is the mass of SgrA*, m is the mass of the IMBH, ρ is the mass density of stars in the central cluster, and $\ln(\Lambda)$ is the

Coulomb logarithm. For circular orbit, this can be rewritten as

$$t_0 = \frac{T_{\text{orb}}}{16\pi^2 \log(\Lambda)} \times \left(\frac{M}{m}\right) \left(\frac{M}{\rho r^3}\right), \quad (14)$$

where T_{orb} is the orbital period of the IMBH. Genzel et. al. (2003) have measured the density profile of the central cusp to be

$$\rho \simeq 10^6 (r/10'')^{-1.3} M_{\odot} \text{pc}^{-3}. \quad (15)$$

For a realistic IMBH $M/m \sim 1000$. Therefore for the stars located a few arcseconds from SgrA* the relevant inspiral timescale is between a few hundred and a few thousand orbital periods. In our simulations we use fiducial values of the mass ratio $M/m = 1000$ and the inspiral timescale of one thousand initial orbital periods of the IMBH. Our inspiral timescale remains constant over the simulation run; this approximation would be exact if the cusp density profile scaled as $\rho \propto r^{-1.5}$ (see e.g. Appendix of Gould and Quillen, 2003). We spot-check our results by varying the inspiral timescale and making sure that our qualitative conclusions do not change.

3.2. Circular inspiral.

Figure 1 shows a pictorial representation of a typical circular inspiral. The points (x, y) on the figure represent ten thousand snapshots of the x and y coordinate of the star. The orthogonal rotating axis x and y belong to the inspiral plane and are chosen so that the SgrA* and IMBH are always on the x axis. From Figure 1 we can trace the dynamical history of the star as the inspiral proceeds. Initially the star is bound to the IMBH which is climbing towards the center on the x -axis. Then the tidal field of SgrA* disrupts the star-IMBH binary, the star escapes from the IMBH via the inner Lagrange point and spends some time inside of the IMBH orbit. Then as a result of a close encounter, the star is flung outside of the IMBH orbit. The star then continues to have encounters with the IMBH, and its eccentricity and inclination get kicks during the encounters. Eventually, the orbit of the IMBH is shrunk enough so that the encounters do not occur any more and the star's eccentricity and inclination stay virtually constant. Figure 2 and 3 show how the star's eccentricity and inclination evolve with time.

Using CITA's Mackenzie cluster, we have performed one thousand simulation runs, such as the one shown in Figures 1, 2, and 3. The initial conditions were different for each run; we have chosen the stars in all the runs to have the same initial Jacoby integral. In Figure 4 we show in the (e, i) plane the scatter plot of the final eccentricities and inclinations. Because of multiple close encounters, the orbits are highly chaotic: even a slight change in the initial conditions or in the timestep of the integrator leads, after some time, to a very different trajectory and thus to a different final eccentricity and inclination relative to the inspiral plane. One subtle issue is the choice of timestep⁶. Usually, one can make sure that the chosen timestep is appropriate by running the simulation with the fraction of the chosen timestep and checking if the simulation results stays the same. In our case however, the system is chaotic and the individual trajectory will always be different after some time if a different integration timestep is chosen. However, it is not the individual trajectories that we are after; rather, we want to know what *distribution* of the orbital parameters one should expect in the inspiral scenario. Therefore, we have repeated the 1000 runs with the same initial conditions but with the timestep

of 0.3 of the original timestep, and checked if the two sets of (e, i) points could belong to the same two-dimensional distribution. The first thing to check was whether the averages agreed; they did. However, we wanted a more complete test. For one-dimensional data, Kolmogorov-Smirnov test is both popular and mathematically well justified. For two-dimensional data, there exist only semi-empirical algorithms based on Monte-Carlo simulations: see Peacock (1983) and Fasano and Franceschini (1987). We used the procedure outlined in the latter to check whether the two (e, i) data sets were compatible with the same distribution; they were.

The remarkable thing about the scatter plot in Fig. 4 is that while the stars, on average, end up with significant eccentricity, more than 99% of them have inclinations smaller than 10 degrees. We make another 1000 runs with the inspiral rate reduced by a factor of 10, we find that while the average eccentricity has increased significantly, and the distribution of inclinations remains similar, with only a few greater than 10 degrees.

3.3. Eccentric inspiral.

The final inclinations are no longer small when the inspiraling IMBH is on an eccentric orbit. Qualitatively, eccentric stellar orbits experience secular torque if the semimajor axes of the star and IMBH are misaligned. Hence angular momentum, inclination, and eccentricity of the star can experience substantial secular changes during the course of the inspiral. In Figure 5 we plot a fraction of stars with inclinations greater than 10 degrees for a few values of IMBH eccentricity. Each point of the graph is obtained by simulating 100 stellar orbits, and the stars which become unbound from SgrA* are removed from the data set. In Figure 6, we show average inclination of stellar orbits after the inspiral, for the same values of IMBH eccentricity. In Figure 7, we show the scatter plot of final inclinations and eccentricities of stars for the case when the IMBH eccentricity is 0.6; the scatter plot contains 1000 points. We observe two groups of unejected stars which are roughly equal in size. In one group, the inclinations are less than 10 degrees, and in another the inclinations are spread evenly between 10 and 180 degrees. In Figures 8 and 9 we show the time evolution of inclination and eccentricity for a typical star which ends up with high inclination.

4. DISCUSSION AND COMPARISON WITH THE DATA.

Current kinematic data indicates that there are two nearly orthogonal stellar discs in the Galactic Center. One of the discs consists of clockwise-moving stars at $\sim 0.1 pc$ from the Black Hole, and has dispersion in inclinations no larger than 10 degrees (Levin and Beloborodov 2003, Genzel et. al. 2003). Some of the stars in this clockwise disc have significant eccentricities (Beloborodov and Levin, 2005). The second disc consists of stars which move counter-clockwise (Genzel et. al. 2003) and its thickness has not been estimated yet; however it is probably thicker than the clockwise disc since the planar fit to its stellar velocity vectors has a large χ^2 of 3.5. The mini-cluster IRS13 with a putative IMBH belongs to this second, thicker disc.

In our simulations the circular inspiral nicely reproduces the kinematics of the thin clockwise disc: dispersion of inclinations is less than 10 degrees yet some of the stars possess significant eccentricities. However, the nearly circular inspiral would never produce the second population of stars which

⁶Here we mean the timestep $d\tau$ in the extended phase space; see the previous section.

move counter-clockwise. Eccentric inspiral seems to be more promising: while significant fraction of stars remain close to the inspiral plain, the rest of the stars get pushed out of the inspiral plain and end up with large inclinations; see Figures 5 and 7. However, the stars with large inclinations do not have a preferred orbital orientation, thus it is hard to imagine them assembling a second disc. Upcoming observations will better constrain the thickness of the second disc and then it will become possible to make a more quantitative assessment of how likely it is to produce the observed counter-clockwise trajectories by an IMBH inspiraling through the plane of the clockwise disc. It seems certain, though, that an IMBH in a counter-clockwise moving IRS13 would not be able to produce the thin clockwise disc. Thus the presence of IMBH in IRS13 could not account for kinematics for all of the young stars at ~ 0.1 pc from SgrA*.

The IMBH in IRS13 would also have difficulty generating highly compact eccentric orbits of the most central stars like SO-2 or SO-16 (see Ghez et. al. 2005). These stars' apoapses are an order of magnitude closer to SgrA* than IRS13. Such disparity of stellar and IMBH orbits is never observed in our simulations. However, we note from Figure 9 that in the case of an eccentric inspiral, the test bodies with high inclination undergo secular evolution in which their eccentricity reaches values close to 1, and their distance of closest approach to the central Hole is much smaller than their semimajor axis. Thus, if such a test body were a binary, this binary could get disrupted by SgrA*, and one of the components of the binary could remain tightly bound to SgrA*. The binary-disruption scenario for formation of the SO-stars was already proposed by Gould and Quillen (2003) in a different context.

We thank Scott Tremaine for introducing us to symplectic integrators in the extended phase space, and Carlo Contaldi for showing us how to use the CITA McKenzie cluster. We have benefited from discussions with Andrei Beloborodov, Jeremy Goodman, Brad Hansen, Chris Matzner, Milos Milosavljevic, and especially with Norm Murray. Our research was supported by NSERC.

APPENDIX: IMBH ECCENTRICITY EVOLUTION DURING THE INSPIRAL.

The orbit of an IMBH in the Galactic Center shrinks due to dynamical friction, and its eccentricity may also evolve with time. The details of this evolution depend on the structure of the stellar cusp surrounding the Black Hole. It is instructive and convenient to model the cluster by a collection of stars of mass m_* with an isotropic distribution function

$$f(r, v) = \beta E^\gamma, \quad (16)$$

where $E = GM/r - v^2/2$ is the binding energy of the star, and β and γ are real numbers. For a Keplerian orbit, the angular momentum and binding energy are given by $L = \sqrt{GMa(1-e^2)}$ and $E = 0.5GM/a$, respectively; here e is the eccentricity of the

orbit. From these relations it is straightforward to derive the evolution equation for IMBH eccentricity:

$$\frac{d \log e}{dt} = -\frac{1-e^2}{2e^2} \left\langle \frac{d \log E}{dt} + 2 \frac{d \log L}{dt} \right\rangle. \quad (17)$$

Here the symbol $\langle \rangle$ represents averaging over the orbital period. The acceleration from dynamical friction acting on the IMBH with velocity vector \vec{v} is given by the Chandrasekhar formula

$$\vec{a} = -k\vec{v}, \quad (18)$$

where

$$k = \frac{4\pi G^2 m_* m \log \Lambda}{v^3} \int_0^v du \times 4\pi u^2 f(r, u). \quad (19)$$

Therefore,

$$\langle dE/dt \rangle = \langle kv^2 \rangle, \quad (20)$$

and

$$\langle dL/dt \rangle = -\langle k \rangle L; \quad (21)$$

cf. Eqs (A5) and (A6) of Gould and Quillen (2003). It is convenient to perform orbital averaging by expressing all the quantities through the mean anomaly ϕ :

$$\begin{aligned} r &= a(1 - e \cos \phi), \\ v^2 &= \frac{GM}{a} \frac{1 + e \cos \phi}{1 - e \cos \phi}, \\ dt/T_{\text{orb}} &= (1 - e \cos \phi) \frac{d\phi}{2\pi}. \end{aligned} \quad (22)$$

After some algebra, one gets

$$\frac{d \log e}{d \log a} = -\frac{1-e^2}{2e^2} (k_1/k_2 - 1), \quad (23)$$

where

$$k_1 = \int_0^1 x^2 dx \int_0^{2\pi} d\phi [1 - (1 + e \cos \phi)x^2]^\gamma (1 - e \cos \phi)^{1-\gamma}, \quad (24)$$

and

$$k_2 = \int_0^1 x^2 dx \int_0^{2\pi} d\phi [1 - (1 + e \cos \phi)x^2]^\gamma (1 - e \cos \phi)^{-\gamma} (1 + e \cos \phi). \quad (25)$$

We evaluate the integrals numerically and in Fig. 10 we plot $-d \log e / d \log a$ as a function of eccentricity, for $\gamma = -0.2$ and $\gamma = 0.25$. The two values of γ correspond to the observed density profile $\rho \propto r^{-1.3}$ and the Bahcall-Wolf density profile $\rho \propto r^{-1.75}$. We see from the graphs that in both cases eccentricity changes by a factor less than 2 as the semimajor axis shrinks by 3 orders of magnitude. Hence, in our simulations we are justified in keeping the eccentricity of IMBH orbit constant.

REFERENCES

- Alexander, T., & Livio, M. 2004, 606, L21
Duncan, M. J., Levison, H. F., & Lee, M. H. 1998, AJ, 116, 2067
Fasano, G., & Franceschini, A. 1987, MNRAS, 225, 155
Genzel, R., et. al. 2000, MNRAS, 317, 348
Genzel, R., et. al. 2003, ApJ, 594, 812
Gerhard, O. 2001, ApJ, 546, L39
Ghez, A. M., et. al. 2003, ApJ, 586, L127
Ghez, A. M., et. al. 2005, to appear in ApJ (astro-ph/0306130)
Goodman, J., & Tan, J. C. 2004, ApJ, 608, 108
Gould, A., & Quillen, A. C. 2003, ApJ, 592, 935
Gurkan, M. A., Freitag, M., & Rasio, F. A. 2004, ApJ, 604, 632
Gurkan, M. A., & Rasio, F. A. 2004, submitted to ApJ (astro-ph/0412452)

- Hansen, B. M. S., & Milosavljevic, M. 2003, *ApJ*, 593, L77
- Jaroszynski, M. 2000, *AcA*, 50, 67
- Kim, S. S., Figer, D. F., & Morris, M. 2004, *ApJ*, 607, L123
- Kolykhalov, P. I., & Sunyaev, R. A. 1980, *SvAL*, 6, 357
- Levin, Y., & Beloborodov, A. M. 2003, *ApJ*, 590, L33
- Levin, Y. 2003, *astro-ph/0307084*
- Maillard, J. P., et. al. 2004, *A&A*, 423, 155
- McMillan, S. L. W., & Portegies Zwart, S. F. 2003, *ApJ*, 596, 314
- Mikkola, S. 1997, *CeMDA*, 67, 145
- Mikkola, S., & Tanikawa, K. 1999, *CeMDA*, 74, 287
- Mikkola, S., & Wiegert, P. 2002, *CeMDA*, 82, 375
- Milosavljevic, M., & Loeb, A. 2004, *ApJ*, 604, L45
- Morris, M., Ghez, A. M., & Becklin, E. E. 1999, *Advances in Space Research*, 23, 959
- Nayakshin, S., Cuadra, J., & Sunyaev, R. 2004, *A&A*, 413, 173
- Peacock, J. A. 1983, *MNRAS*, 202, 615
- Phinney, E. S. 1989, *The Center of the Galaxy* (136th symposium of the IAU, edited by M. Morris), 543
- Portegies Zwart, S. F., et. al. 2004, *Nature*, 428, 724
- Preto, M., & Tremaine, S. 1999, *AJ*, 118, 2532
- Sanders, R. H. 1998, *MNRAS*, 294, 35
- Schodel, R., et. al. 2002, *Nature*, 419, 694
- Schodel, R., et. al. 2003, *ApJ*, 596, 1015
- Shlosman, I., & Begelman, M. 1987, *Nature*, 329, 810
- Yu, Q., & Tremaine, S. 2003, *ApJ*, 599, 1129

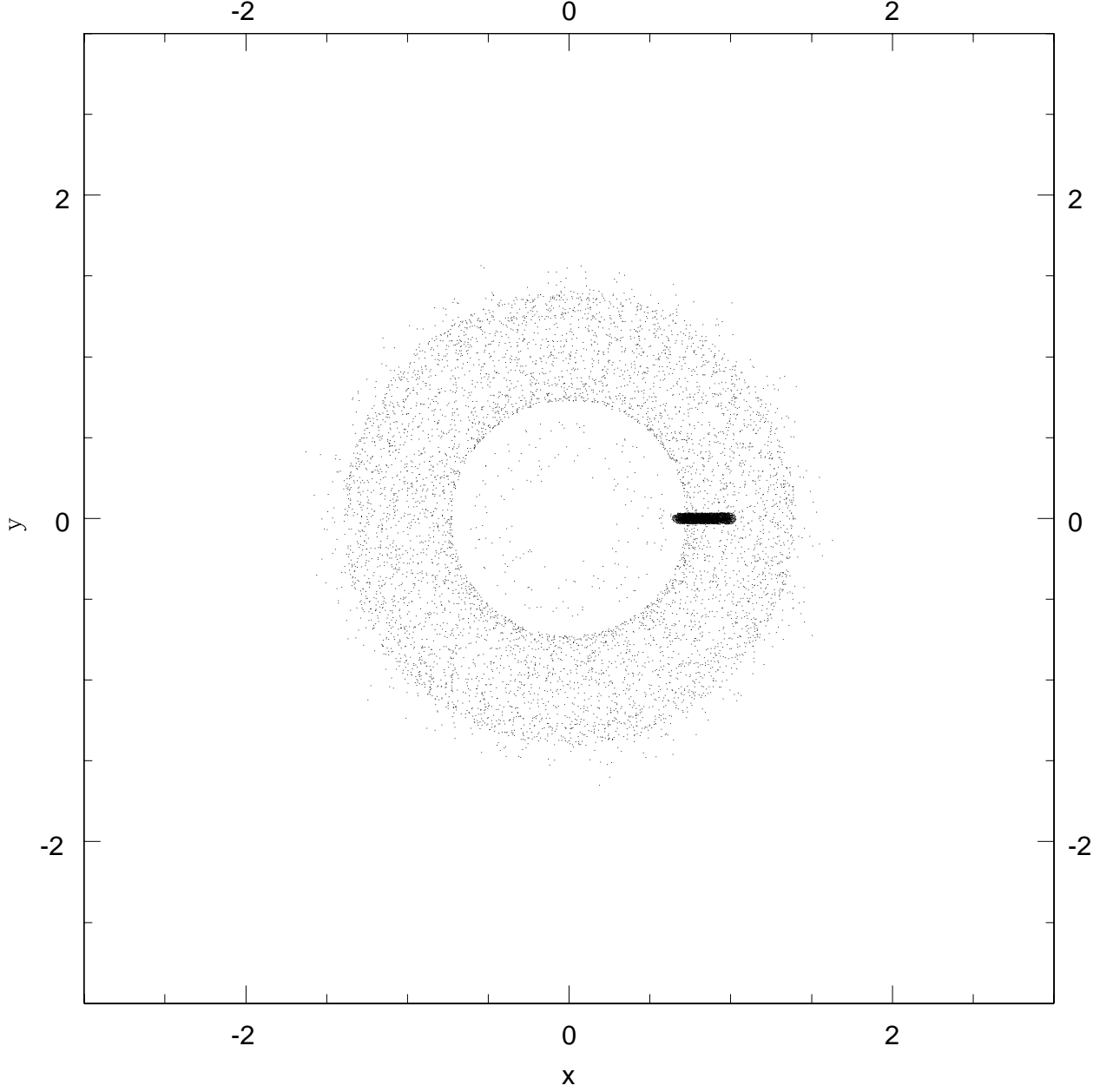


FIG. 1.— 10000 snapshot of the stellar position in the IMBH inspiral plane. Rotating coordinates axes are chosen so that both IMBH and SgrA* are on the x -axis, and their origin coincides with the baricenter. The star is originally bound to the IMBH; this corresponds to the dense dark region of the scatter plot. The star escapes through the inner Lagrange point, then gets flung outside by a close encounter with the IMBH. A few close encounters follow, and then the orbit stabilises once the black-hole binary is shrunk away from the stellar periaipse. Units on x and y axes are arbitrary.

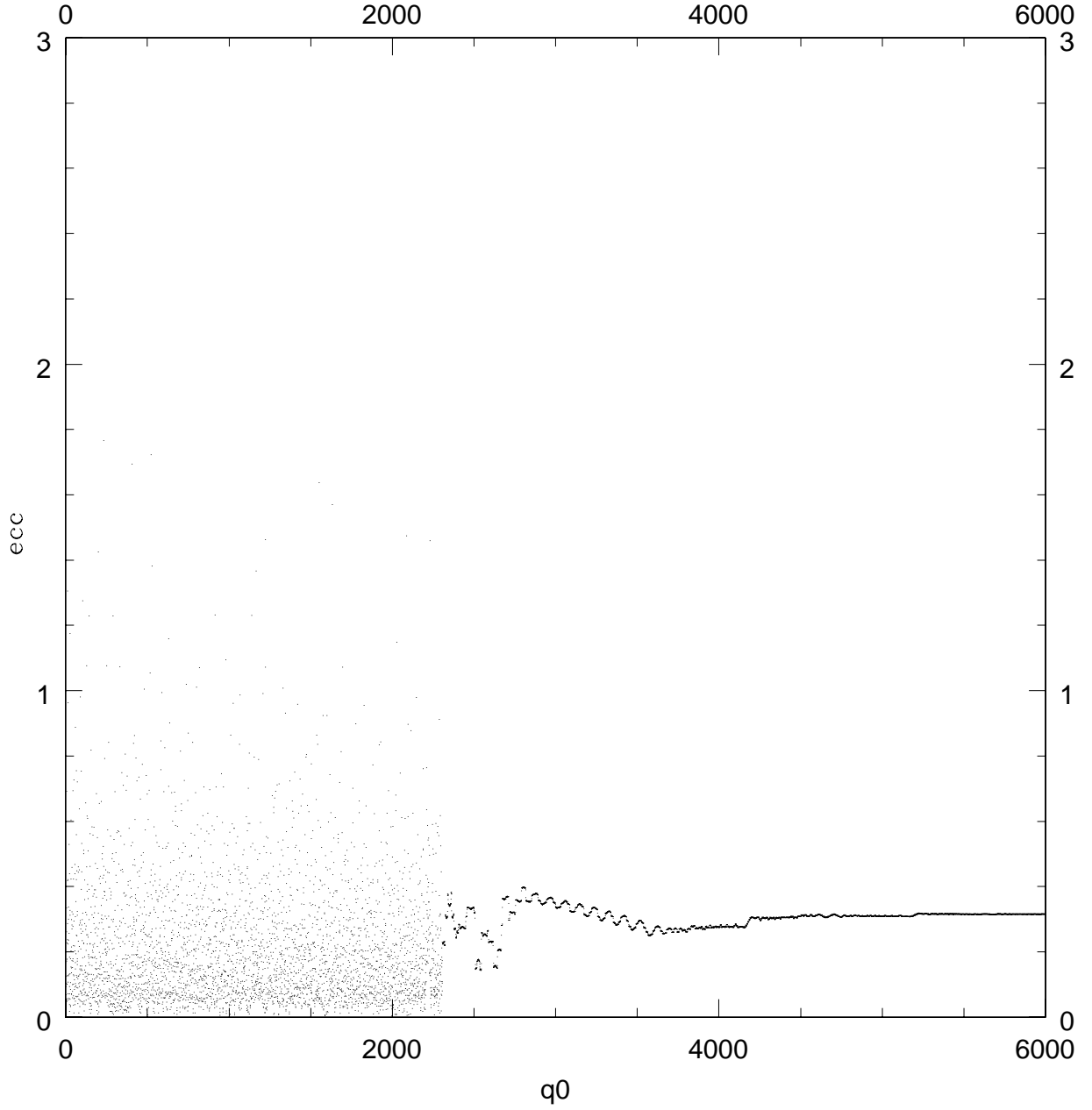


FIG. 2.— 10000 snapshots of eccentricity evolution for the star in Figure 1. The eccentricity is evaluated relative to the baricenter. When the star is bound to the IMBH and comes close to it, the eccentricity relative to the baricenter may become greater than 1. Time units: initial IMBH orbital period is 2π .

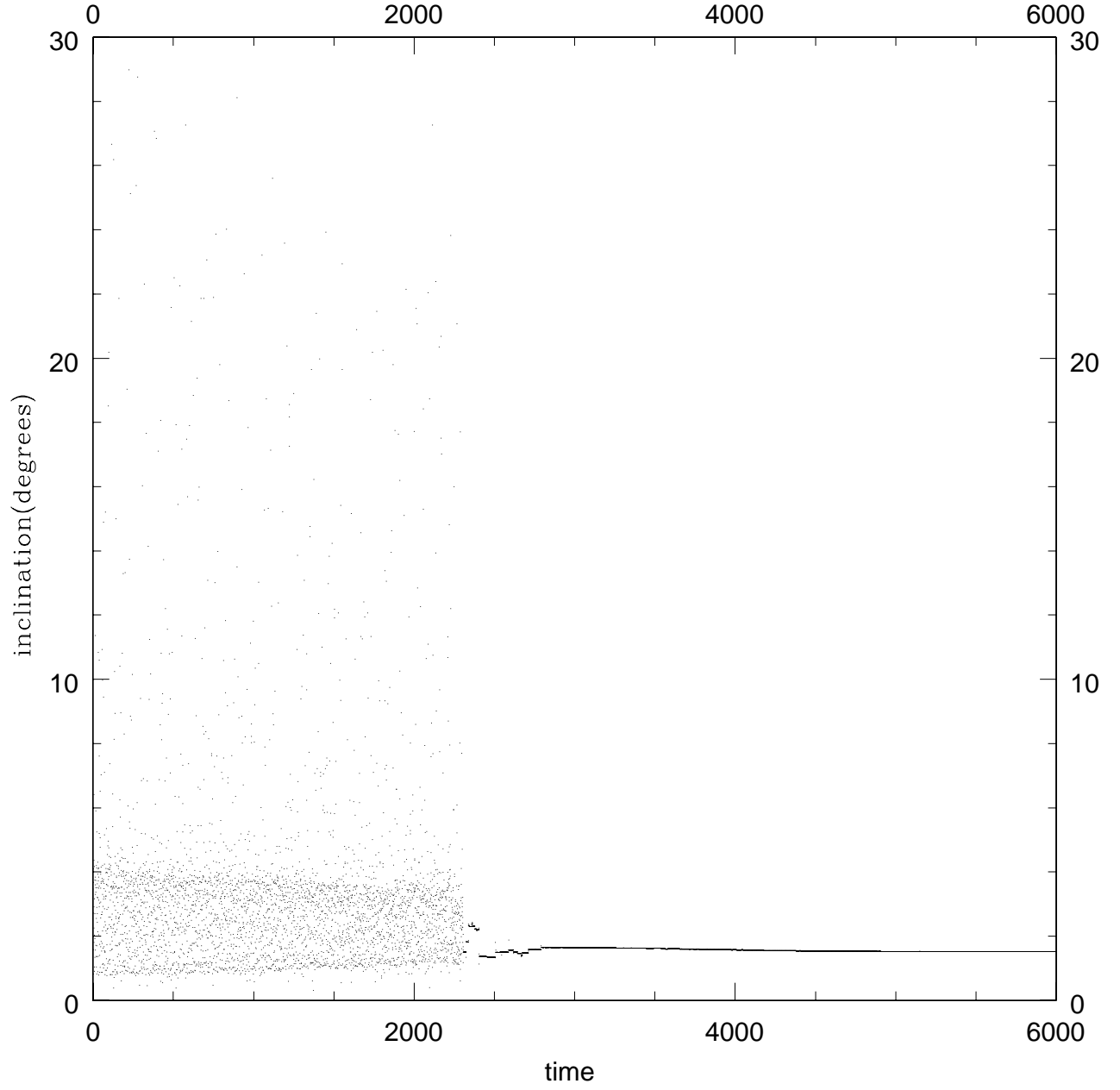


FIG. 3.— 10000 snapshots of inclination evolution for the star in Figure 1. The inclination is evaluated relative to the baricenter. When the star is bound to the IMBH and comes close to it, the inclination relative to the baricenter may become large. Time units: initial IMBH orbital period is 2π .

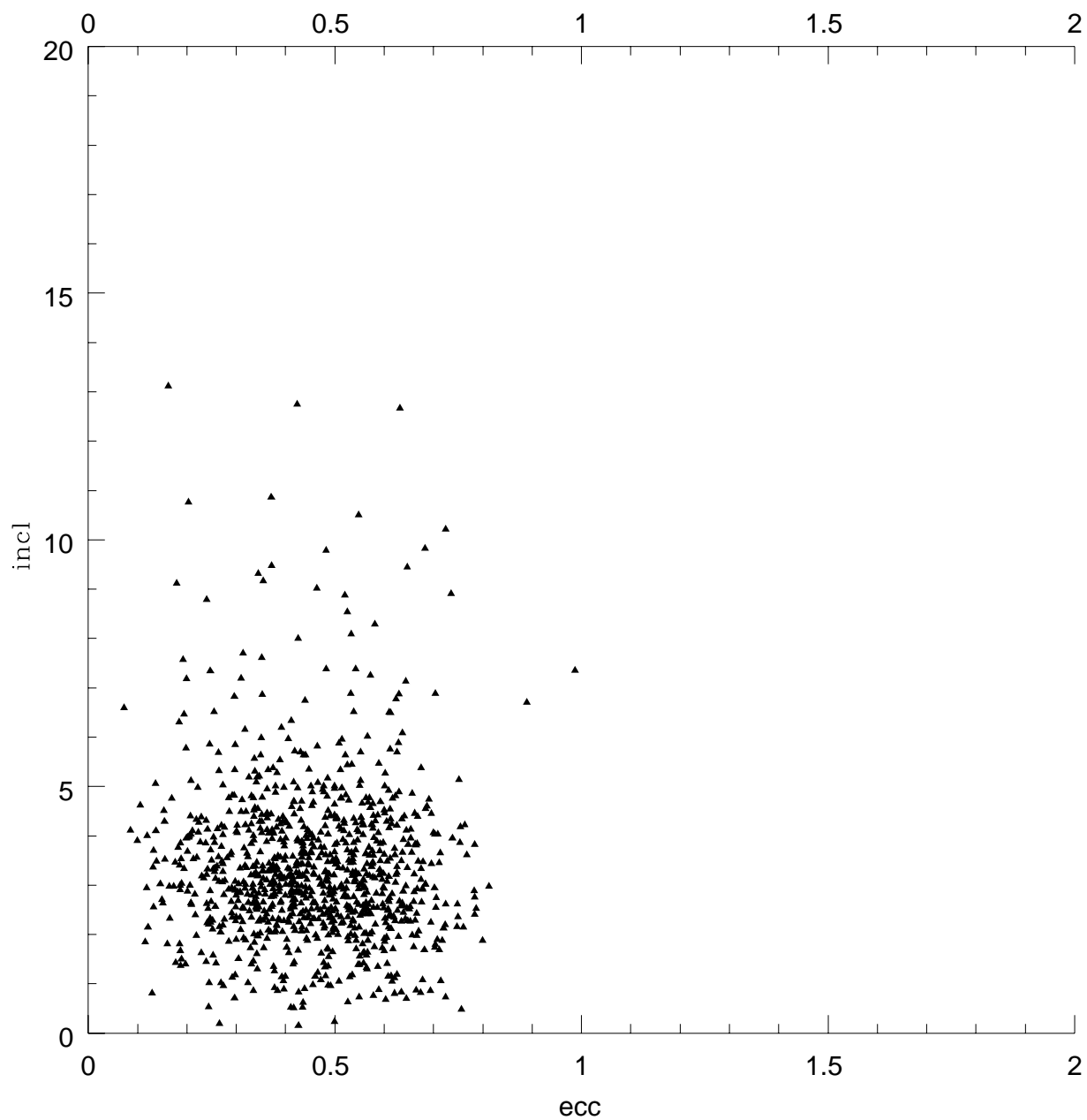


FIG. 4.— Scatter plot of eccentricities and inclinations for a thousand stars after a circular inspiral.

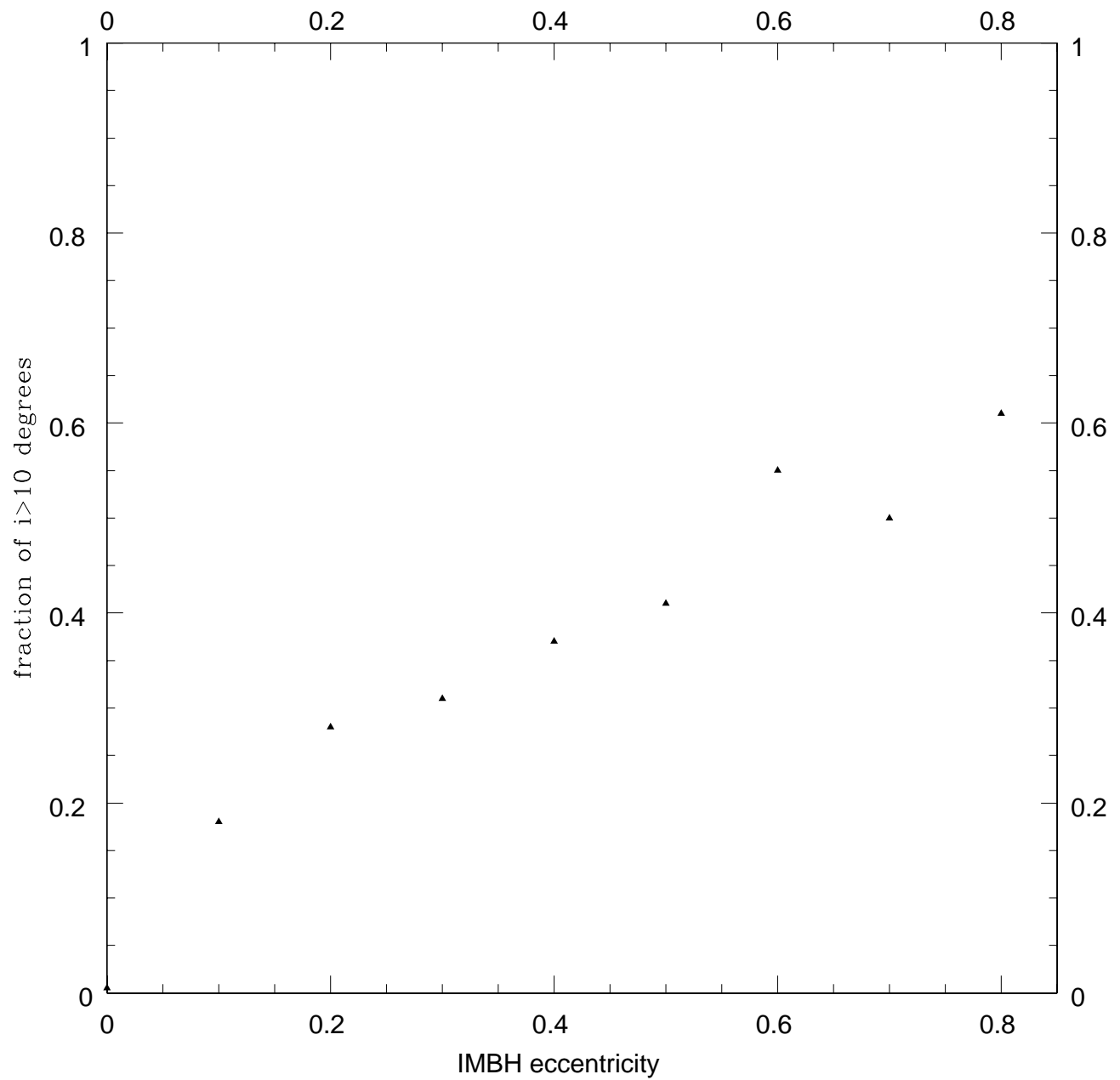


FIG. 5.— A fraction of stars with inclination > 10 degrees plotted vs IMBH eccentricity. Each point is obtained from 100 runs.

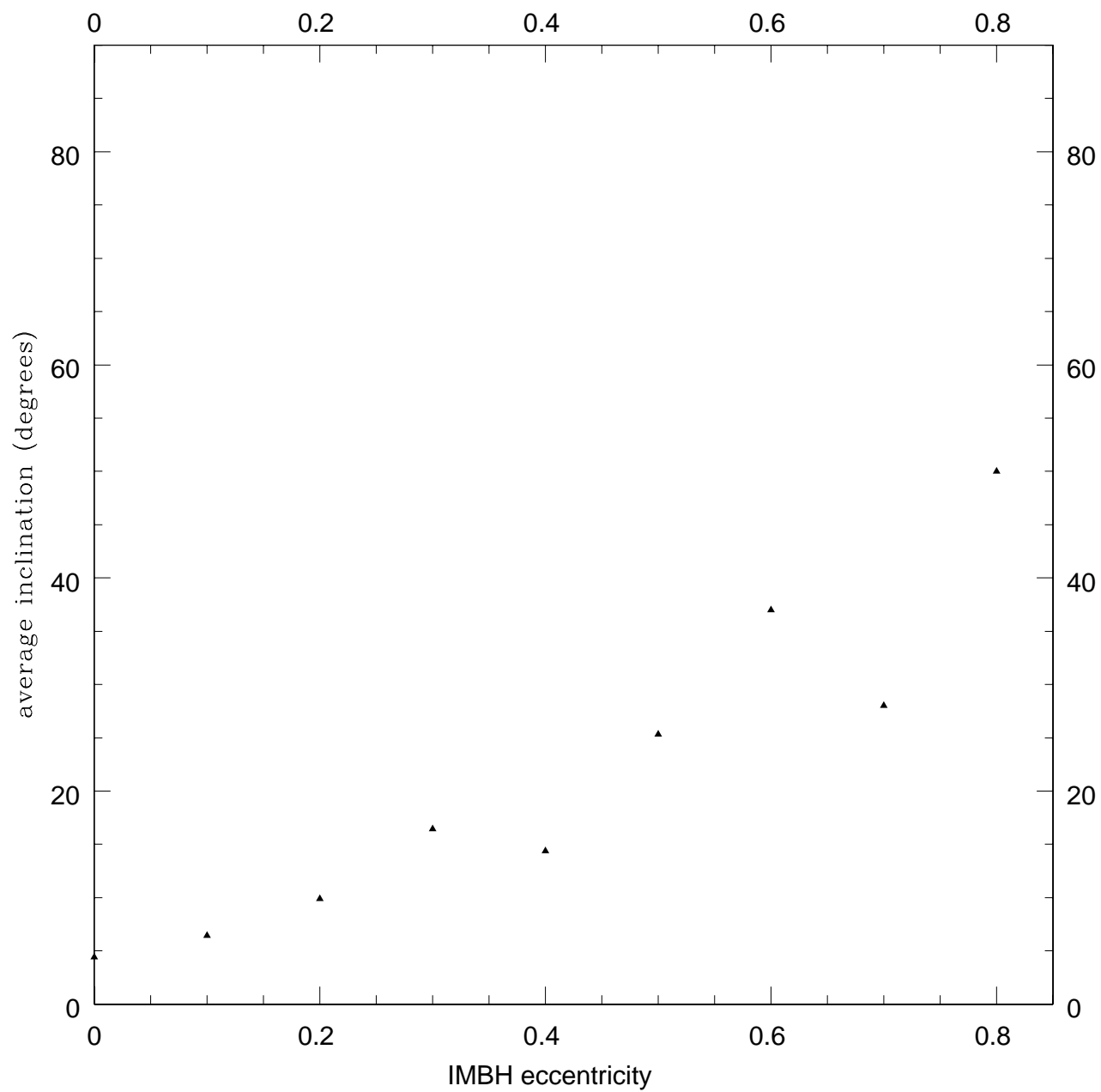


FIG. 6.— Average inclination plotted vs IMBH eccentricity. Each point is obtained from 100 runs.

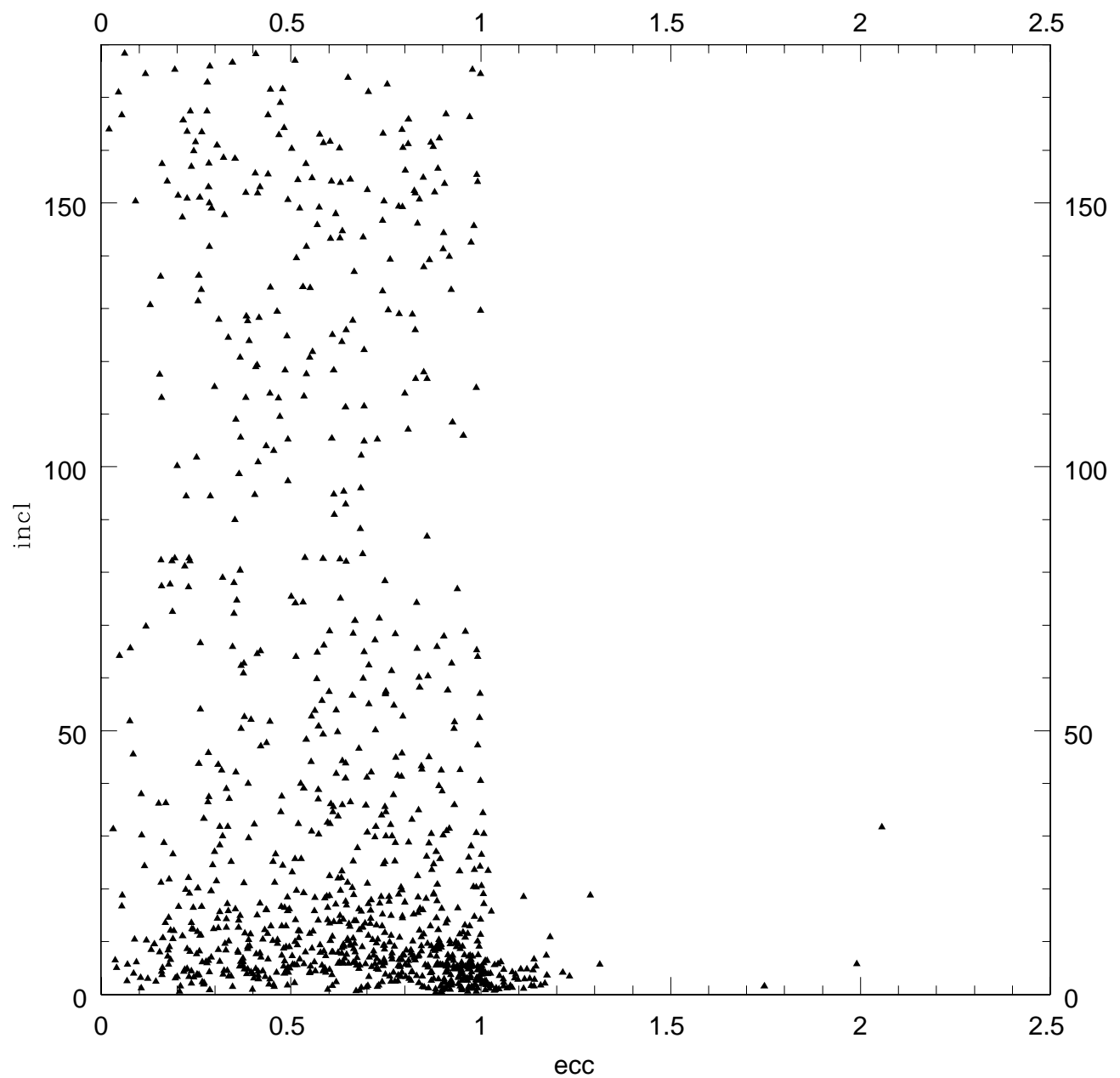


FIG. 7.— Scatter plot of eccentricities and inclinations for a thousand stars after an inspiral with IMBH eccentricity of 0.6.

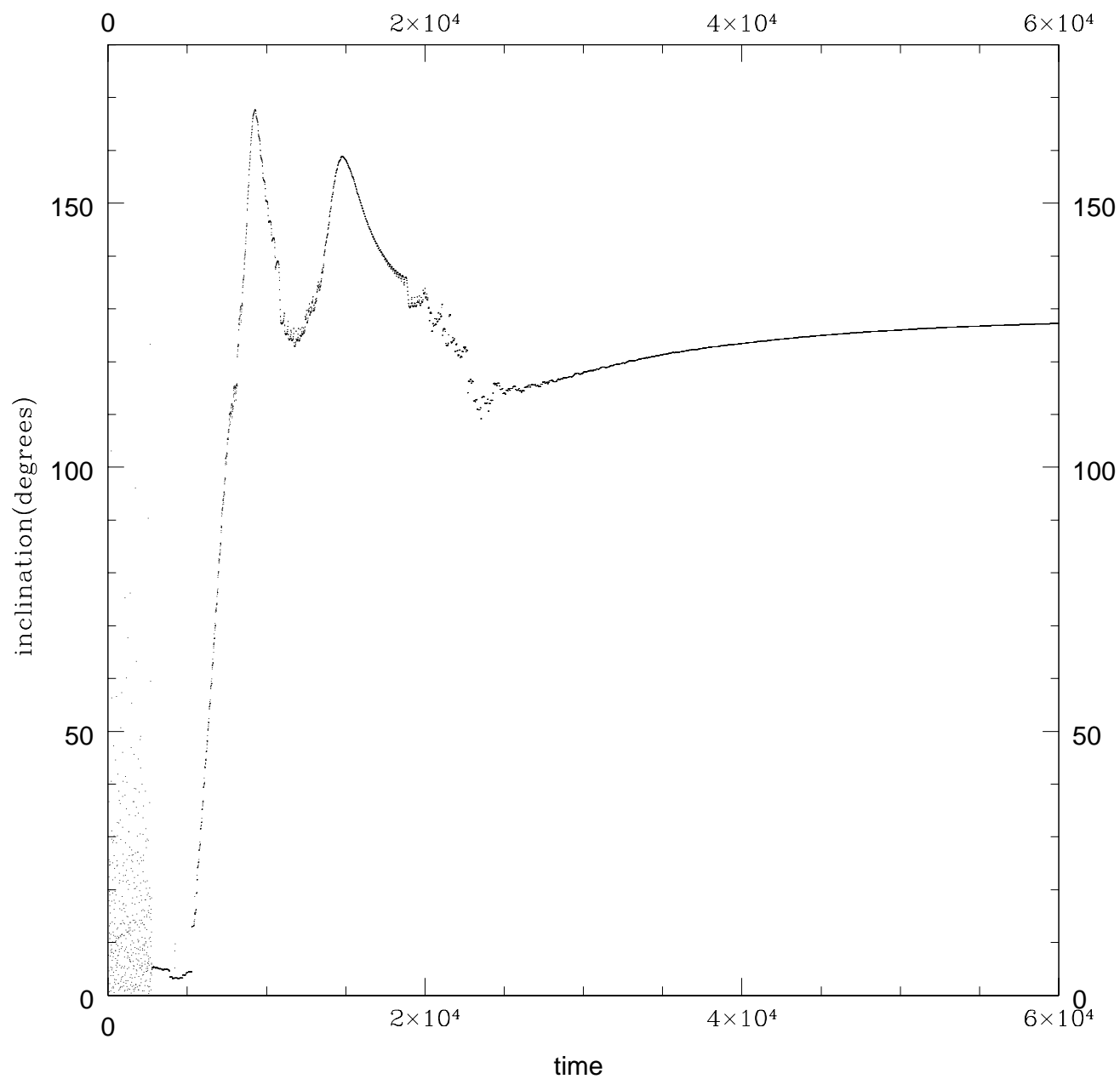


FIG. 8.— Inclination evolution of a typical high-inclination star; IMBH eccentricity is 0.6

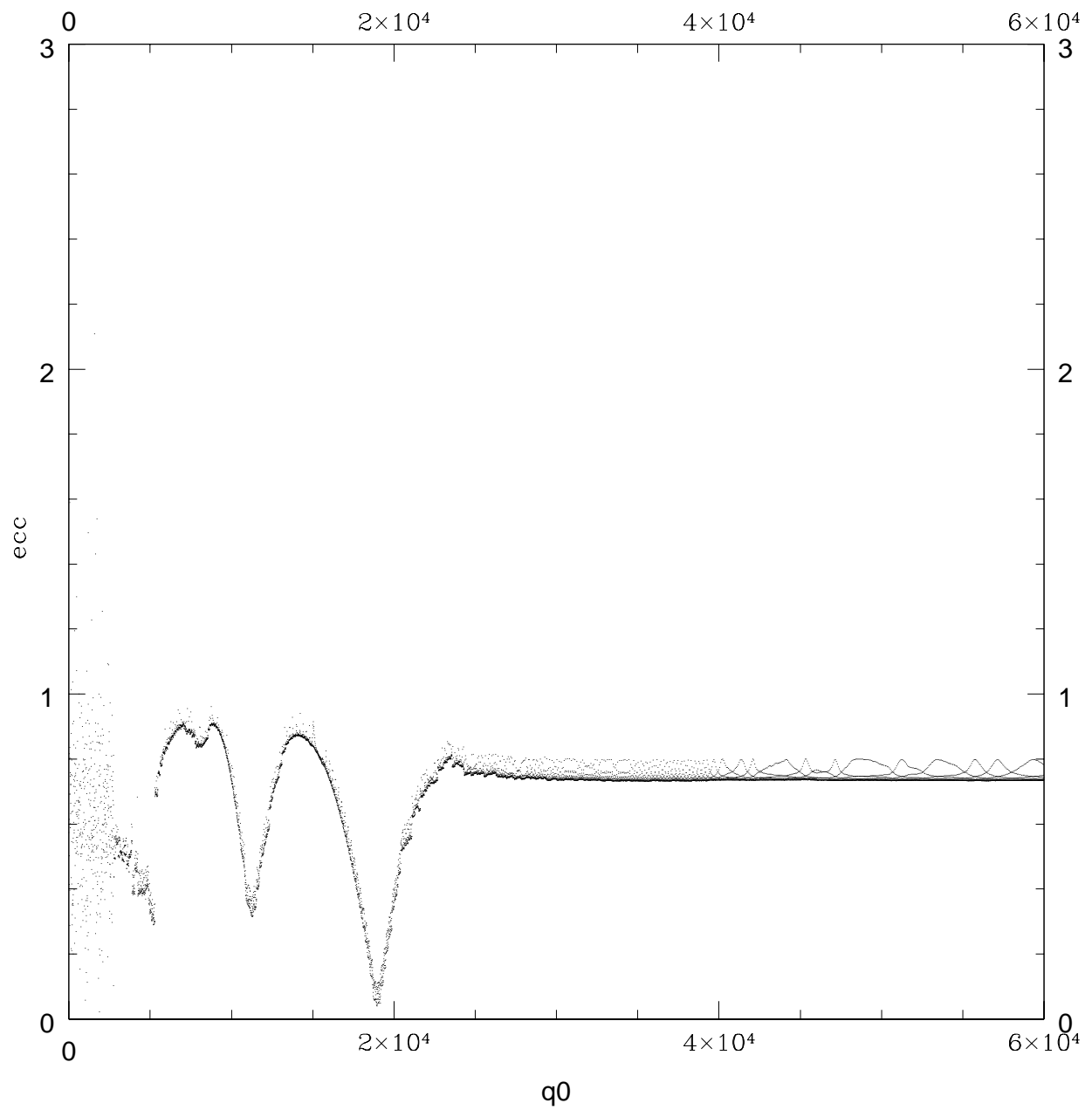


FIG. 9.— Eccentricity evolution of the same high-inclination star as in Figure 8.

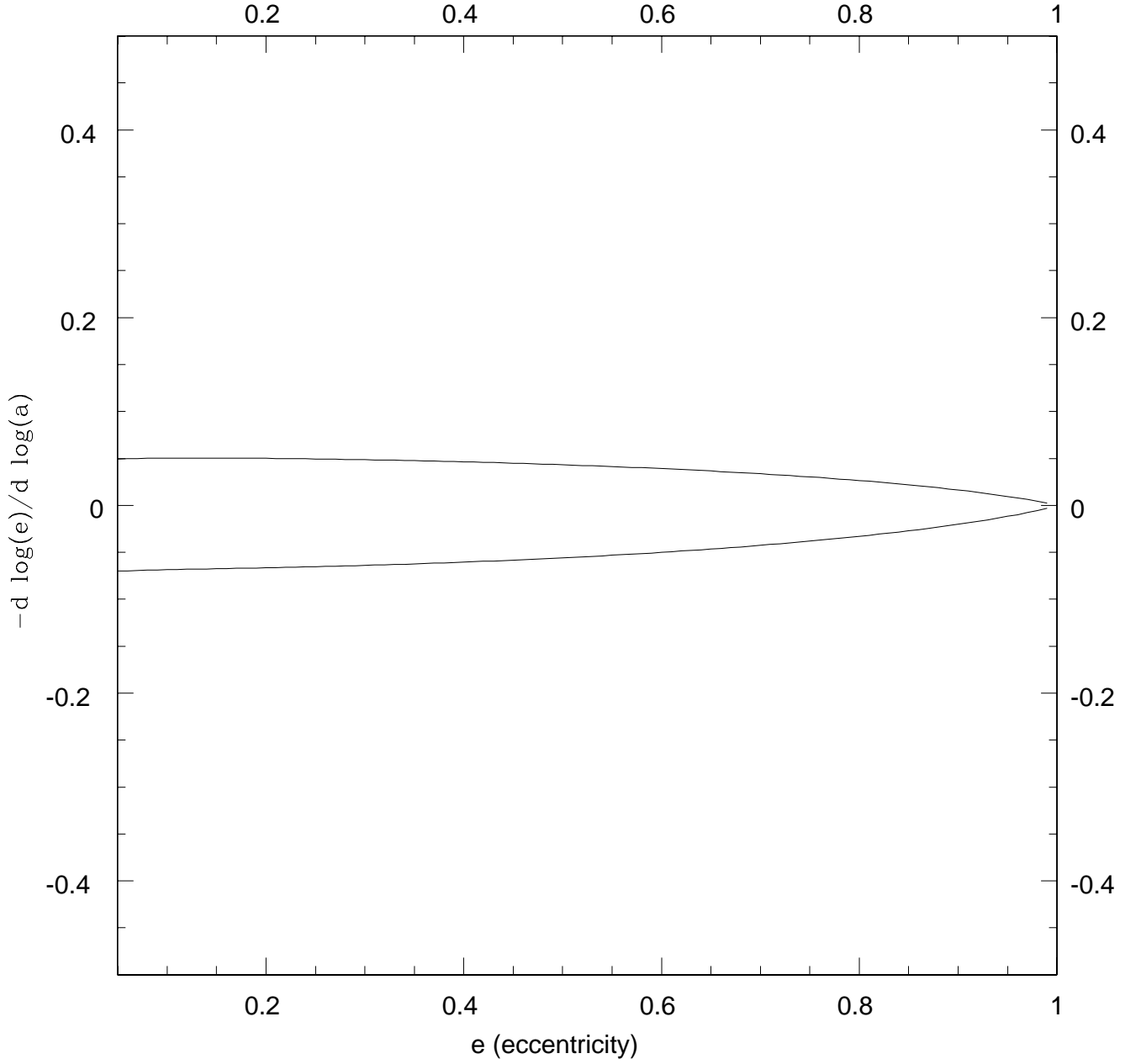


FIG. 10.— Plot of the IMBH eccentricity growth rate $d \log e / d \log(1/a)$ vs e . Upper curve is computed for the observed density profile of luminous matter in the Galactic Center, $\rho \propto r^{-1.3}$, and lower curve is computed for a relaxed Bahcall-Wolf density profile, $\rho \propto r^{-1.75}$.